Laboratory of Quantum Computing and Information

Luca Menti
(Dated: July 13, 2023)

The purpose of this report is to illustrate the experimental techniques and results obtained from two distinct laboratory experiments. The primary objective of the first experiment is to demonstrate the violation of Bell's inequality in CHSH form, named after the scientific team who derived it: John Clauser, Michael Horne, Abner Shimony, and Richard Holt. The intent of the second experiment, on the other hand, is to reconstruct the density matrix of a quantum system. This is achieved through quantum state tomography, using two different derivations: linear inversion and maximum likelihood estimation.

CHSH INEQUALITY VIOLATION

Purpose of the experience

The EPR theory, named after its contributors Albert Einstein, Boris Podolsky, and Nathan Rosen, posits that there are essential elements of reality lacking in the incomplete theory of quantum mechanics. John Bell's famous inequality emerged as an empirical test of the EPR theory. Experimental evidence showed that various quantum systems violated Bell's inequality, undermining the completeness of the theory and introducing new paradigms for understanding the concept of entanglement.
The primary objective of this laboratory experiment is to showcase the violation of the CHSH form of Bell's inequality. This will be achieved by recording coincidence counts in the polarization measurements of photons.

Theory explanation

In Bell's hypothetical scenario, a pair of particles is prepared and sent to two different individuals, Alice and Bob. Both Alice and Bob have access to two distinct measurement devices, allowing them to measure different physical properties. For instance, Alice can measure properties $\hat{A_0}$ and $\hat{A_1}$, while Bob can measure $\hat{B_0}$ and $\hat{B_1}$. These properties can only yield outcomes of either $+1$ or -1. It is assumed that the measurement outcomes represent inherent characteristics of the particles, which are merely revealed through the act of measurement. Alice and Bob have the freedom to independently and randomly select which physical property to measure, as long as their measurements occur simultaneously. The condition is crucial to ensure that Alice's measurement does not influence Bob's result, and vice versa. By incorporating the principles of locality (which states that the influence of an event is limited to the speed of light) and the existence of hidden variables (variables that cannot be observed through experiments but can definitively predict the outcome if known), it becomes possible to perform a correlation measurement referred to as an inequality (CHSH inequality).

$$|\langle\hat{A_0}\otimes\hat{B_0}\rangle+\langle\hat{A_0}\otimes\hat{B_1}\rangle+\langle\hat{A_1}\otimes\hat{B_0}\rangle-\langle\hat{A_1}\otimes\hat{B_1}\rangle| = |\langle\hat{S}\rangle| \leq 2 \quad (1)$$

However, according to quantum mechanics, it is anticipated that in a two-qubit system experiencing a state of complete entanglement, such as, $|\psi\rangle = \frac{1}{\sqrt{2}}(|01\rangle - |10\rangle)$ for instance, with $\hat{A_0} = \vec{a_0}\cdot\vec{\sigma}$, $\hat{B_0} = \vec{b_0}\cdot\vec{\sigma}$, $\hat{A_1} = \vec{a_1}\cdot\vec{\sigma}$, $\hat{B_1} = \vec{b_1}\cdot\vec{\sigma}$, with , $\vec{\sigma} = (\sigma_x, \sigma_y, \sigma_z)$ where $\sigma_{x,y,z}$ are Pauli matrices [2] and $|\vec{a_i}| = |\vec{b_i}| = 1$, the (1) satisfies:

$$|\langle\hat{S}\rangle| = |\langle\psi|(\vec{a}\cdot\vec{\sigma})\otimes(\vec{b}\cdot\vec{\sigma})|\psi\rangle| = |-\vec{a}\cdot\vec{b}| \quad (2)$$

Furthermore, we obtain $|\langle\hat{S}\rangle| \leq 2\sqrt{2}$, considering $a_1 = (0,0,1)$, $b_1 = \frac{1}{\sqrt{2}}(-1,0,-1)$, $a_2 = (1,0,0)$ and $b_2 = \frac{1}{\sqrt{2}}(-1,0,1)$, that is a violation of CHSH inequality. The particles sent to the detectors of this experiment are pairs photons and the entanglement is achieved through spontaneous parametric down conversion (Fig. 1) by handling polarization degrees of freedom of photons. The notation is the following:

$$|D\rangle = \frac{1}{\sqrt{2}}(|H\rangle + |V\rangle) \quad (3)$$

$$|A\rangle = \frac{1}{\sqrt{2}}(|H\rangle - |V\rangle) \quad (4)$$

$$|R\rangle = \frac{1}{\sqrt{2}}(|H\rangle + i|V\rangle) \quad (5)$$

$$|L\rangle = \frac{1}{\sqrt{2}}(|H\rangle - i|V\rangle) \quad (6)$$

where $|V\rangle = \begin{pmatrix}0\\1\end{pmatrix}$ represents linear vertical polarization state and $|H\rangle = \begin{pmatrix}1\\0\end{pmatrix}$ represents the horizontal one. The linear diagonal and anti-diagonal polarization states are in (3) and (4) whereas the circular right and left in (5) and (6).

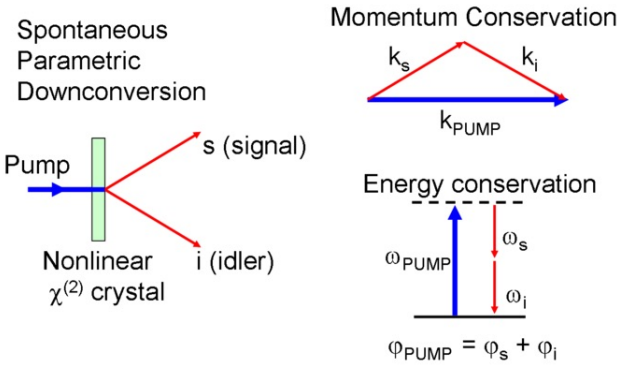

FIG. 1: **Spontaneous Parametric Downconversion.** Spontaneous parametric down-conversion is a phenomenon where a single photon striking a nonlinear crystal can produce two output photons with a probability of $10^{-2} \div 10^{-3}$. This process is dependent upon the conservation of phase and energy of light striking the medium and, two types of phase matching may occur.

In spontaneous parametric down conversion the single incident pumped photon :

$$|\psi\rangle_p = \frac{1}{\sqrt{2}}(|V\rangle_p + |H\rangle_p) \tag{7}$$

turns into a pair of entangled signal and idler photons:

$$|\psi\rangle_{s,i} = \frac{1}{\sqrt{2}}(|VV\rangle_{s,i} + |HH\rangle_{s,i}) \tag{8}$$

and considering the basis $\{|V\rangle, |H\rangle\}$ it is possible to compute:

$$p_{VV} = |\langle VV|\psi\rangle_p|^2 = \frac{1}{2} \tag{9}$$

$$p_{VH} = |\langle VH|\psi\rangle_p|^2 = 0 \tag{10}$$

$$p_{HV} = |\langle HV|\psi\rangle_p|^2 = 0 \tag{11}$$

$$p_{VV} = |\langle HH|\psi\rangle_p|^2 = \frac{1}{2} \tag{12}$$

which are the probabilities for the different events. To ensure the presence of entanglement it is necessary to compute :

$$p_{AA} = |\langle AA|\psi\rangle_p|^2 = \frac{1}{2} \tag{13}$$

$$p_{AD} = |\langle AD|\psi\rangle_p|^2 = 0 \tag{14}$$

$$p_{DA} = |\langle DA|\psi\rangle_p|^2 = 0 \tag{15}$$

$$p_{DD} = |\langle HH|\psi\rangle_p|^2 = \frac{1}{2} \tag{16}$$

that are the probabilities linked to the complementary basis $\{|A\rangle, |D\rangle\}$. [3]

As concerned the wave plates (that have optical axis parallel to the horizontal direction of polarization), their action on a single state of photon is represented by the following operator:

$$M = \begin{pmatrix} e^{-\frac{i\Gamma}{2}} & 0 \\ 0 & e^{\frac{i\Gamma}{2}} \end{pmatrix} \tag{17}$$

In particular for the quarter and half wave Γ is equal to $\frac{\pi}{2}$ and π respectively.

Usign the rotation matrix $R(\theta)= \begin{pmatrix} cos(\theta) & -sin(\theta) \\ sin(\theta) & cos(\theta) \end{pmatrix}$ wave plates can be rotated w.r.t the horizontal direction of polarization by an angle θ. The operator (17) becomes:

$$M_\theta = R(\theta) \cdot M \cdot R(-\theta) \tag{18}$$

Instrumental apparatus and measurement methodology

A continuously emitting laser beam at $405nm$ wavelength passes through an eyepiece to maintain its shape and clarity. The beam is then focused to the requisite position of the non-linear crystal. After reflecting off two mirrors, it traverses a half wave plate (HWP), which alters the polarization of the light and creates a superposition of polarization states. The beam then proceeds through a non-linear crystal, resulting in spontaneous parametric down-conversion (SPDC) and producing pairs of entangled photons as depicted in Fig. 1.
For type II phase matching, the entanglement of photons is automatic, given that the generated photons are indistinguishable and have an intrinsic ambiguity in their position. They remain in two different cones and are symmetrical in relation to their middle position. Conversely, for type I phase matching, entanglement involves two different crystals with orthogonal optical axes which require pumping photons in a superposition of polarizations. In this instance, the pairs of photons are generated at a probability of 10^{-6} (Fig. 2).
At this point, the photon pairs pass through birefringent crystals that compensate for any time delays between the

creation of the pairs. The pairs then pass through several sets of eyepieces, lenses, and mirrors, before reaching the measurement apparatus where an effective measurement is made.

The measurement device utilized in this experiment consists of a sequence of optical components, including a quarter wave plate (QWP), a half wave plate (HWP), and a polarizing beam splitter (PBS). The wave plates are used to change the measurement's basis, while the PBS only transmits horizontally polarized light, reflecting the vertically polarized component.

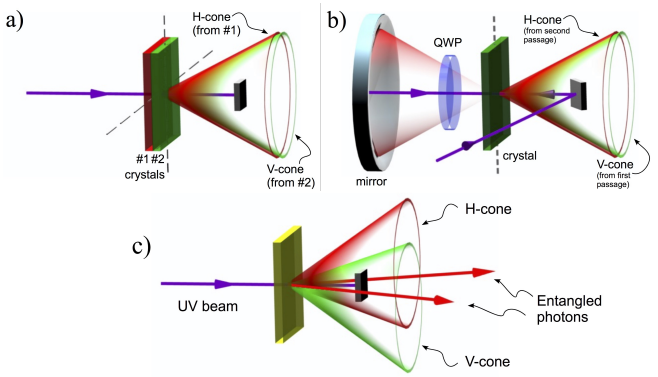

FIG. 2: **Different types phase matching.** Type I phase matching (a and b) and Type II phase matching (c). In type I phase matching, two photons with identical polarization are generated, whereas in type II phase matching, the generated photons possess orthogonal polarization.

Afterward, interference filters are used to select only the pumped light with a wavelength centered at $810nm$ with a bandwidth of $10nm$, cleaning the beam from the background light. The experiment (Fig. 3) was conducted in complete darkness to minimize all possible interference and noise sources. The beam is then focused by a lens and sent through a multimode fiber to the Geiger-like detectors (Alice and Bob), which detect the arrival of a photon and convert this information into an electric signal created by an avalanche mechanism due to the photon impacting on a silicon apparatus. The delay between the actual arrival of the photon and the creation of the output signal is approximately $1ns$. The electric signal travels through a TTL cable and is sent to a time-to-digital converter, which compares the time of arrival of the signal with its own clock period of 80,955ps. This device is linked to a computer that generates text files including two columns. The first column contains the signal's time of arrival in time bins unit, while the second column records the channel in which the signal was detected. In this case, the possible channels are two: channel 1 and 4, corresponding to receivers Alice and Bob.

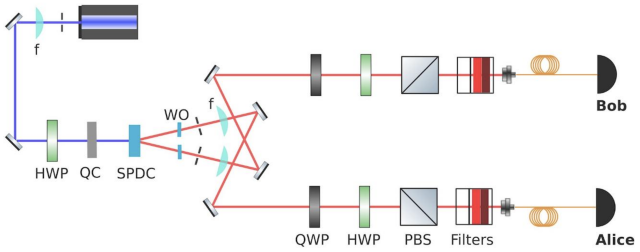

FIG. 3: **Experimental apparatus.** Schema of apparatus used in the experience.

Methods

The text files with collected data are made of two columns:

- one with the photons' arrival time;
- one with the channel where the signal has been measured.

There are 16 different text files since it is possible to decide the acquisition time and to repeat the acquisition for each choice of measurement basis for Alice and Bob and for each possibility of obtained outcomes. For each file only the first second of acquisition has been considered since for higher times there were unexpected features in the timetags.

Initially the arrival time's information has been converted into seconds; in order to do this each time has been multiplied by the duration of one time bit unit $t_{unit} = 80,955ps$ so:

$$t_s = t_{collected} \cdot t_{unit} \tag{19}$$

After this time transformation, the minimum acquisition time across all text files has been found and all the records beyond this limit has been removed. This has been done in order to compare different text files which could lead to unbalance coincidence counts due to different acquisition times otherwise. Then the information about coincident events', that is an indicator of the entanglement between photons, has been extracted. It is important underlying that signals are almost never detected perfectly simultaneously since there is background noise, detectors' limited efficiency, and other experimental limits, so it is necessary to define an "experimental simultaneity", by defining when signals coming from two channels can be considered coincident. For the defining coincidence's time window purpose histograms of coincidence have been used; these histograms represent the frequency of Δt_i which is the time difference between one measurement and the following one. In particular :

$$\Delta t_i = |\Delta t_i| \cdot \Delta CH_i \tag{20}$$

where $|\Delta t_i| = t_{i+1} - t_i$ (time difference two following measurements) and ΔCH_i is the difference between two following detection channels defined as:

$$\Delta CH_i = \begin{cases} -1 & \text{if } \Delta CH_{i+1} - \Delta CH_i < 0 \\ 1 & \text{if } \Delta CH_{i+1} - \Delta CH_i \geq 0 \end{cases}$$

Δt_is are represented pretty well by a normal distribution centered in 0 as shown in the histograms, thereby fitting the experimental distributions with a Gaussian $N(\mu, \sigma^2)$ it is possible to obtain the delay between two channels. This delay is defined as μ while T ,the estimation of the coincidence window, is defined as 4σ. In particular compute the mean across of all these delays, obtained from each text file, allow to get an unique value for the delay. Hence, the coincident events in each text file are counted as the number of following events with different channels and $T > |\Delta t_i|$.
The errors δN_i associated to coincidince counts N_i are expected to adhere to a Poisson distribution since the coincidence counts are rare events compared to the total amount of data collected:

$$\delta N_i = \sqrt{N_i} \tag{21}$$

From the counts probabilities are computed for each choice of basis measurement and for each obtained outcome. Considering $\{|H\rangle, |V\rangle\}$ on Alice and Bob's sides, for instance, the probabilities computed are [4]:

$$p_{HH} = \frac{N_{HH}}{N_{HH} + N_{VH} + N_{HV} + N_{VV}} \tag{22}$$

$$p_{HV} = \frac{N_{HV}}{N_{HH} + N_{VH} + N_{HV} + N_{VV}} \tag{23}$$

$$p_{VH} = \frac{N_{VH}}{N_{HH} + N_{VH} + N_{HV} + N_{VV}} \tag{24}$$

$$p_{VV} = \frac{N_{VV}}{N_{HH} + N_{VH} + N_{HV} + N_{VV}} \tag{25}$$

while the errors are computed by Gaussian errors' propagation formula [5]

$$\delta_{p_{HH}} = \frac{\sqrt{N_{HH}} \cdot \sqrt{N_{HV} + N_{VH} + N_{VV}}}{(N_{HH} + NVH + N_{HV} + N_{VV})^{\frac{3}{2}}} \tag{26}$$

Remanding that the outputs of measurement can only be equal to ± 1 and denoting A_0 and B_0 the choice of $\{|H\rangle, |V\rangle\}$ basis on Alice and Bob's side respectively and with A_1 and B_1 the choice of $\{|D\rangle, |A\rangle\}$ basis, the expected value of the observable for A_0 and B_0 (for example) is :

$$E_{A_0,B_0} = p_{HH} + p_{VV} - p_{HV} - p_{VH} \tag{27}$$

and the error (computed again using Gaussian errors' propagation formula):

$$\delta_{E_{A_0,B_0}} = 2 \cdot \sqrt{\frac{(N_{HV} + N_{VH}) \cdot (N_{HH} + N_{VV})}{(N_{HH} + N_{VV} + N_{VH} + N_{HV})^3}} \tag{28}$$

Same consideration can be done for the other choices of basis.

Hence, the experimental value for (2) is:

$$S_e = E_{A_0,B_0} + E_{A_0,B_1} + E_{A_1,B_0} - E_{A_1,B_1} \tag{29}$$

and the error:

$$\delta_{S_e} = \sqrt{\delta^2_{E_{A_0,B_0}} + \delta^2_{E_{A_0,B_1}} + \delta^2_{E_{A_1,B_0}} + \delta^2_{E_{A_1,B_1}}} \tag{30}$$

Data Analysis

Before discussing the experimental results obtained, it is important to first address the calibration of the Half-Wave Plates (HWPs) and determine the rotational angles ϕ_0 at which the plates align their optical axes vertically. Two dataset containing registered counts in function of the waveplate angle have been considered. The data have been fitted using Malus' Law (with an addition of a scaling factor in *cos* argument):

$$I = I_0 \cdot cos^2(2 \cdot (\phi - \phi_0)) + \epsilon \tag{31}$$

where:

- I is the intensity (counts in this case)
- I_0 is the initial intensity
- ϕ waveplate angle
- ϕ_0 waveplate reference angle
- ϵ the offset

The fit has been performed considering the *scipy.optimize* library in Python and the *minimize* function. The algorithm's initialising parameters were: ϕ corresponding to the angle with the minimum number of coincidences, I_0 equal to the difference between the highest number of coincidences' counts and the lowest one and ϵ which corresponds to the minimum number of coincidences' counts. The results are shown in table I and in Fig 4.

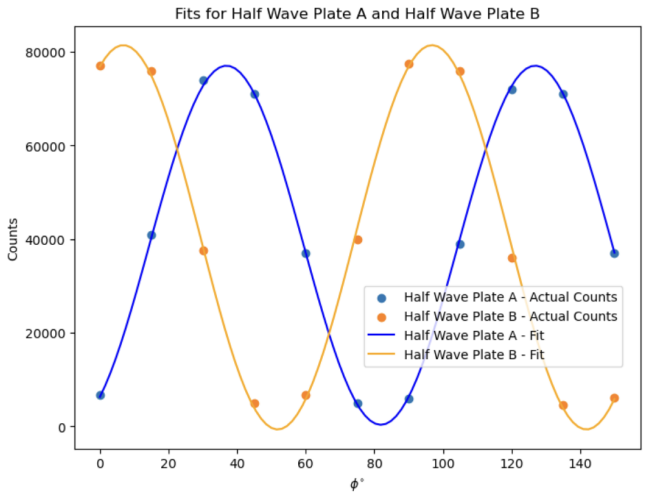

FIG. 4: **Fits for Half Wave Plate A and Half Wave Plate B.** Fits for two dataset containing registered counts in function of the waveplate angle in order to find the optimized rotational angles ϕ_0.

HPW	I_0	ϕ_0	ϵ
A	76720	36.9°	346
B	82104	96.8°	-650

TABLE I: Parameters obtained from the fits.

After calculating the optimized rotational angles ϕ_0, the serie of rotational angles remains constant. Hence the following experimental operations with the subsequent data collected has got predefined and calibrated configurations. Furthermore this angles' computation allows a rigorous polarization states' handling and control which is useful for other investigations and for obtaining the results hoped for. After this preliminary computation, it is possible to move to the calculation of S_e.
First of all the the records with a time acquisition greater than $1s$ have been discarded. Since the coincidence events are pretty rare the time differences considered are in the interval $[-7 \cdot 10^{-9}s, 7 \cdot 10^{-9}s]$. As expained before, the histograms of Δt_i have been fitted with a Gaussian distribution (Fig. 5) and the results for the different fits are shown in Tab. II.
All μ are on the order of nanoseconds, showing that there is not an higher delay between 2 channels, which is equal to the mean of μ obtained: $\overline{\mu}$=-5.37 ns. As concern the coincidence time window it has been considered $T = 4\sigma$. Once obtained the time window it was possible to count the events N_{counts} the related error, probabilities p and probabilities uncertainties, as described in eq. (21-26). The results are reported in Tab. III.

Operator and Outcome	A	$\mu(ns)$	$\sigma(ns)$
A_0,+1 B_0, +1	2534	-5.33	0.38
A_0,-1 B_0, -1	2446	-5.38	0.43
A_0,-1 B_0, +1	511	-5.35	0.44
A_0,+1 B_0, -1	647	-5.38	0.37
A_1,+1 B_0, +1	2782	-5.37	0.39
A_1,-1 B_0, -1	2462	-5.38	0.44
A_1,-1 B_0, +1	530	-5.36	0.37
A_1,+1 B_0, -1	576	-5.39	0.45
A_0,+1 B_1, +1	10760	-5.38	0.43
A_0,-1 B_1, -1	10795	-5.39	0.39
A_0,-1 B_1, +1	432	-5.37	0.39
A_0,+1 B_1, -1	478	-5.4	0.4
A_1,+1 B_1, +1	773	-5.37	0.38
A_1,-1 B_1, -1	612	-5.37	0.42
A_1,-1 B_1, +1	2522	-5.39	0.39
A_1,+1 B_1, -1	2638	-5.39	0.39

TABLE II: Gaussian fits' parameters for different textfiles.

Operator and Outcome	N_{counts}	$\delta_{N_{counts}}$	p	δp
A_0,+1 B_0, +1	9230	96	0.390	0.003
A_0,-1 B_0, -1	9906	100	0.419	0.003
A_0,-1 B_0, +1	2100	46	0.089	0.001
A_0,+1 B_0, -1	2408	49	0.102	0.001
A_1,+1 B_0, +1	10367	102	0.417	0.003
A_1,-1 B_0, -1	10176	101	0.410	0.003
A_1,-1 B_0, +1	1950	44	0.077	0.001
A_1,+1 B_0, -1	2386	49	0.096	0.001
A_0,+1 B_1, +1	10739	104	0.430	0.003
A_0,-1 B_1, -1	10812	104	0.433	0.003
A_0,-1 B_1, +1	1612	40	0.064	0.001
A_0,+1 B_1, -1	1812	43	0.073	0.001
A_1,+1 B_1, +1	2821	53	0.1150	0.0007
A_1,-1 B_1, -1	2471	50	0.1011	0.0007
A_1,-1 B_1, +1	9381	97	0.384	0.001
A_1,+1 B_1, -1	9773	99	0.400	0.001

TABLE III: Coincidence counts and probabilities with the respective errors for the different combinations of basis and operators.

Suddenly it was possible to compute the expected value of the measured observable and the associated errors using eq. (27) and (28) (Tab. IV).

	E	δE
E_{A_0,B_0}	0.618	0.005
E_{A_1,B_0}	0.654	0.005
E_{A_0,B_1}	0.726	0.004
E_{A_1,B_1}	-0.568	0.005

TABLE IV: Expected value of measured observables.

Finally S_e and the error were computed using (29-30):

$$S_e = 2.57 \pm 0.01 \tag{32}$$

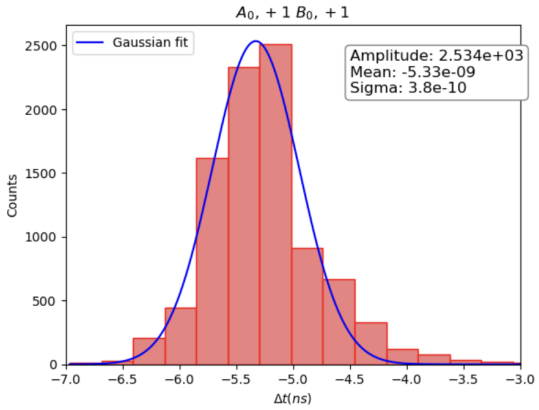

FIG. 5: **Example of fitted histogram.** A graphical representation showing the frequency distribution of time intervals Δt_i, which has been modeled using a Gaussian distribution. This histogram pertains to the operators A_0 and B_0, and specifically focuses on the outcomes where both operators yield a result of +1.

Conclusion

The value obtained in (32) proves the violation of Bell's inequality as expected from literature experimental results.

QUANTUM STATE TOMOGRAPHY

Purpose of the experiment

The objective of this experiment is to reconstruct the density matrix, which characterizes the collection of photons, employing two distinct methodologies.
The first approach involves deriving the density matrix through a linear transformation of experimental data. However, it is important to note that due to experimental noise, the resulting state may not adhere to positive semidefiniteness, rendering it non-physical.
In contrast, the second technique utilizes numerical optimization to identify the density matrix that is most likely responsible for the observed data. This approach effectively circumvents the issue of potential non-physical outcomes. Furthermore, additional meaningful quantities such as Fidelity, Von Neumann entropy, and Concurrence have been computed with the associated statistical errors, that have been calculated using a large number of simulated data points.

Theory explanation

The idea behind linear inversion technique is to reconstruct the density matrix $\hat{\rho}$ of a quantum system by measuring state of photons in particular directions.
In order to choose these directions it is enough to turn the angles of half and quarter wave plates directly preceding the detectors. The state corresponding to the projection measurement in one of the beams is described as

$$|\psi_p^{(1)}(h,q)\rangle = \hat{U}_{QWP}(q)\cdot\hat{U}_{HWP}(h)|H\rangle \tag{33}$$

where $\hat{U}_{QWP}(q)\cdot\hat{U}_{HWP}(h)$ is the operator that represents the action of a quarter wave plate where the axis is rotated by an angle $q(h)$ [6].
Hence, the projection state of both photons is:

$$|\psi_p^{(1,2)}(h_1,q_1,h_2,q_2)\rangle = |\psi_p^{(1)}(h_1,q_1)\rangle\otimes|\psi_p^{(2)}(h_2,q_2)\rangle \tag{34}$$

Being $|\psi_\alpha\rangle$ the projection state corresponding to wave plates angles $\{h_{1,\alpha},q_{1,\alpha},h_{2,\alpha},q_{2,\alpha}\}$, the number of expected coincidence counts in a measurement of the state is given by:

$$n_\alpha = A\langle\psi_\alpha|\hat{\rho}|\psi_\alpha\rangle \tag{35}$$

with A costant which depends on flux of photon and efficiency of detector.
It is possible to simply rewriting $\hat{\rho}$ as a linear combination of 16 4x4 matrices linearly indipendent:

$$\hat{\rho} = \sum_{\alpha=1}^{16}\hat{\Gamma}_\alpha r_\alpha \tag{36}$$

where r_α are real parameters and $\hat{\Gamma}_\alpha = \frac{1}{2}\hat{\sigma}_i\otimes\hat{\sigma}_j$ with $\hat{\sigma}_{\{1,2,3\}}$ the Pauli matrices, $\hat{\sigma}_0 = I_{2\times2}$ and $i,j = \{0,1,2,3\}$.
Combing (35) and (36)

$$n_\alpha = A\sum_{\beta=1}^{16}B_{\alpha,\beta}r_\beta \tag{37}$$

with $B_{\alpha,\beta}$ a non singular 16x16 matrix :

$$B_{\alpha,\beta} = \langle\psi_\alpha|\hat{\Gamma}_\beta|\psi_\alpha\rangle \tag{38}$$

Hence, given the non singularity of $B_{\alpha,\beta}$ and inverting (37):

$$r_\alpha = A^{-1}\sum_{\beta=1}^{16}B^{-1}_{\alpha,\beta}n_\beta \tag{39}$$

And substituting (39) into (36):

$$\hat{\rho} = A^{-1}\sum_{\alpha=1}^{16}\hat{M}_\alpha n_\alpha \tag{40}$$

Where $\hat{M}_\alpha$ 4x4 matrices and A are :

$$\hat{M}_\alpha = \sum_{\alpha=1}^{16}B^{-1}_{\alpha,\beta}\hat{\Gamma}_\beta \tag{41}$$

$$A = \sum_{\alpha=1}^{16}Tr\{\hat{M}_\alpha\}n_\alpha \tag{42}$$

and finally the density matrix of the system is:

$$\hat{\rho} = \frac{\sum_{\alpha=1}^{16} \hat{M}_\alpha n_\alpha}{\sum_{\alpha=1}^{16} Tr\{\hat{M}_\alpha\} n_\alpha} \tag{43}$$

The density matrix obtained with linear inversion technique could violate some physical properties (positive semidefiniteness for instance). In order to overcome this problem the technique of maximum likelihood estimation can be used starting from linear inversion result. In this methods it is assumed that $\hat{\rho}$ is physical , i.e.:

- normalized
- Hermitian
- positive semidefinite

so $\hat{\rho}$ is written as a matrix:

$$\hat{\rho}(t) = \frac{\hat{T}^\dagger(t)\hat{T}(t)}{Tr\{\hat{T}^\dagger(t)\hat{T}(t)\}} \tag{44}$$

with $t = \{t_1, ..., t_{16}\}$ real variables and $\hat{T}(t)$ 4x4 triangular matrix [7]:

$$\begin{pmatrix} t_1 & 0 & 0 & 0 \\ t_5 + it_6 & t_2 & 0 & 0 \\ t_{11} + it_{12} & t_7 + it_8 & t_3 & 0 \\ t_{15} + it_{16} & t_{13} + it_{14} & t_9 + it_{10} & t_4 \end{pmatrix} \tag{45}$$

Furthermore it is possible to introduce a likelihood function as a function of t and n_α to understand how well the data are represented by $\hat{\rho}$. Assuming the probability of obtain the experimental data assuming a Gaussian noise for the coincident measurements is:

$$P(n_1, ...n_{16}) = \frac{1}{K} \prod_{\alpha=1}^{16} e^{-\frac{(n_\alpha - \bar{n}_\alpha)^2}{2\sigma_\alpha^2}} \tag{46}$$

where $\bar{n}_\alpha = A\langle\psi_\alpha|\hat{\rho}(t)|\psi_\alpha\rangle$, K is a normalization factor and $\sigma_\alpha = \sqrt{\bar{n}_\alpha}$ due to the fact the coincidence counts are Poissonians. So usign these expression in (46):

$$P(n_1, ...n_{16}) = \frac{1}{K} \prod_{\alpha=1}^{16} e^{-\frac{(n_\alpha - A\langle\psi_\alpha|\hat{\rho}(t)|\psi_\alpha\rangle)^2}{2A\langle\psi_\alpha|\hat{\rho}(t)|\psi_\alpha\rangle}} \tag{47}$$

Maximizing the probability $P(n_1, ..., n_{16})$ or minimizing the likelihood function of exponential's argument it is possible to find the optimal set t_{best} of parameters t:

$$L(t_1, ..., t_{16}) = \sum_{\alpha=1}^{16} \frac{(n_\alpha - A\langle\psi_\alpha|\hat{\rho}(t)|\psi_\alpha\rangle)^2}{2A\langle\psi_\alpha|\hat{\rho}(t)|\psi_\alpha\rangle} \tag{48}$$

By the way it is necessary to provide a set of input value t_{inp} for t. In order to do this it is sufficient to extract the parameters from $\hat{\rho}$ computed before with linear inversion technique:

$$\hat{T} = \begin{pmatrix} \sqrt{\frac{\Delta}{M_{11}}} & 0 & 0 & 0 \\ \frac{M_{12}}{\sqrt{M_{11}M_{11,22}}} & \sqrt{\frac{M_{11}}{M_{11,22}}} & 0 & 0 \\ \frac{M_{12,23}}{\sqrt{\hat{\rho}_{44}M_{11,22}}} & \frac{M_{12,23}}{\sqrt{\hat{\rho}_{44}M_{11,22}}} & \sqrt{\frac{M_{11,22}}{\hat{\rho}_{44}}} & 0 \\ \frac{\hat{\rho}_{41}}{\sqrt{\hat{\rho}_{44}}} & \frac{\hat{\rho}_{42}}{\sqrt{\hat{\rho}_{44}}} & \frac{\hat{\rho}_{43}}{\sqrt{\hat{\rho}_{44}}} & \sqrt{\hat{\rho}_{44}} \end{pmatrix} \tag{49}$$

where $\Delta = Det(\hat{\rho})$, M_{ij} is the first minor of $\hat{\rho}$ i.e.the determinant of the 3x3 matrix formed by deleting the $i-th$ raw and the $j-th$ column of $\hat{\rho}$ and $M_{ij,kl}$ is the second minor of $\hat{\rho}$ i.e. the determinant of the 2x2 matrix formed by deleting the $i-th$ and $k-th$ rows and the $j-th$ and $l-th$ columns of $\hat{\rho}$ ($i \neq k$ and $j \neq l$) .

Finally we can give some measurements:

- Fidelity $F(\hat{\rho}, \hat{\sigma})$, which is a measurament of how much two states $\hat{\rho}$ and $\hat{\sigma}$ are close to each other

$$F(\hat{\rho}, \hat{\sigma}) = F(\hat{\sigma}, \hat{\rho}) = [Tr(\sqrt{\sqrt{\hat{\rho}}\hat{\sigma}\sqrt{\hat{\rho}}})]^2 \tag{50}$$

- Von Neumann entropy S which is a measurament of purity of a state $\hat{\rho}$ (with p_m eigenvalue of $\hat{\rho}$)

$$S = -Tr\{\hat{\rho}log_2(\hat{\rho})\} = -\sum_{m=1}^{4} p_m log_2 p_m \tag{51}$$

- Concurrence C, which is a measurament of quantum coherence properties of a mixed state and for two qubits

$$C = max\{0; \sqrt{r_1} - \sqrt{r_2} - \sqrt{r_3} - \sqrt{r_4}\} \tag{52}$$

with $r_{1,2,3,4}$ eigenvalues of $\hat{R} = \hat{\rho}\hat{\Sigma}\hat{\rho}^T\hat{\Sigma}$ s.t. $r_1 \geq r_2 \geq r_3 \geq r_4$ and $\hat{\Sigma} = \begin{pmatrix} 0 & 0 & 0 & -1 \\ 0 & 0 & 1 & 0 \\ 0 & 1 & 0 & 0 \\ -1 & 0 & 0 & 0 \end{pmatrix}$.

Instrumental apparatus and measurament methodology

The instrumental apparatus is the same described in the previous experiment (Fig. 3). In particular qubits are implemented by manipulating the polarization properties of entangled photons derived from coherent light sources.

Methods

The dataset is made of 16 coincidence counts' measurements in three different projection states:

- $|\phi^+\rangle = \frac{1}{\sqrt{2}}|HH\rangle + |VV\rangle$
- $|\phi^-\rangle = \frac{1}{\sqrt{2}}|HH\rangle - |VV\rangle$
- $|\phi_D\rangle$, the decoherent state

realized moving the wave plates axes in appropriate inclinations angles.
Since some data for $|\phi^+\rangle$ and $|\phi_D\rangle$ were missed they were "rebuilt". In particular the missing coincidence counts C_{missed} where given by:

$$C_{missed} = N_{|\phi^-\rangle} \cdot \frac{\sum_{k=1}^{4} C_k}{\sum_{k=1}^{4} N_{|\phi_k^-\rangle}} \tag{53}$$

with $N_{|\phi^-\rangle}$ counts for $|\phi^-\rangle$ in the missed counts' record and k=1, 2, 3, 4 since they have been considered $\{|VV\rangle, |HH\rangle, |VH\rangle, |HV\rangle\}$ basis' matrices that have unitary traces, so $N_{|\phi_k^-\rangle}$ are the corresponding counts. Then the projective states have been computed as explained in (34) from the measured wave plates angles. Suddenly $\hat{\Gamma}_\alpha$s and $B_{\alpha,\beta}$ have been calculated and the latter one has been inverted. Abruptly $\hat{M}_\alpha$ has been computed (41-42) and inserted in equation (43), leading to the linear inversion density matrix $\hat{\rho}_{LI}$.

Obtained the latter, the eigenvalues have been computed to check the positive semidefiniteness of $\hat{\rho}_{LI}$ itself. Furthermore, knowing the linear inversion density matrix allowed to compute the initial parameters t_i for the maximum likelihood function as explained in equations (45) and (49). Again, with the help of *scipy.optimize* library and the *minimize* function considering the *SLSQP* method the minimization of (48) has been performed; the best parameters obtained from this process have been used in equations (44-45) in order to get the maximum likelihood density matrix $\hat{\rho}_{LKL}$.
In conclusion, Fidelity, Von Neumann entropy and Concurrence have been computed for the two density matrices. The statistical errors for these quantities have been evaluated by simulation, chasing the following path.
First of all each obtained count has been considered as a Poissonian random variable $\mathcal{P}_n(\lambda) = e^{-\lambda}\frac{\lambda^n}{n!}$ with mean value λ equal to the obtained experimental data; then to evaluate the statistical properties of the system, an ensemble of 300 simulated density matrices has been generated using the above statistical distribution. For each simulated density matrix ρ, the Fidelity and Concurrence have been determined as measures of the quality and entanglement, respectively. The statistical errors have been calculated as the standard deviations of the simulated results, providing an estimate of the uncertainties associated with the measurements.

Data Analysis

The data used for the analysis with also the missed counts computed as explained in equation (53) are shown in Tab V, while the wave plates axes' inclination angles are shown in Tab. VI.

$Mode_1$	$Mode_2$	HWPA	QWPA	HWPB	QWPB	$N_{\|\phi^+\rangle}$	$N_{\|\phi^-\rangle}$	$N_{\|\phi_D\rangle}$
H	H	37	47	7	270	5220	9000	16000
H	V	37	47	52	270	270	400	650
V	V	82	47	52	270	5300	9000	17000
V	H	82	47	7	270	314	550	1200
R	H	82	92	7	270	3400	5802	10671
R	V	82	92	52	270	2600	4437	8160
D	V	59.5	92	52	270	3200	5461	10043
D	H	59.5	92	7	270	3050	5205	9572
D	R	59.5	92	7	225	3300	5632	10357
D	D	59.5	92	29.5	225	300	8700	15000
R	D	82	92	29.5	225	3200	5461	10043
H	D	37	47	29.5	225	2380	4062	7470
V	D	82	47	29.5	225	3500	5973	10985
V	L	82	47	52	225	2400	4096	7532
H	L	37	47	52	225	3000	5120	9416
R	L	82	92	52	225	320	8500	15000
L	L	37	92	52	225	5400	9216	16948

TABLE V: Dataset for quantum state tomography with the $N_{|\phi^+\rangle}$,$N_{|\phi^-\rangle}$ and $N_{|\phi_D\rangle}$ coincidence counts' measurements in three different states.

Mode1	Mode2	HWPA	QWPA	HWPB	QWPB
H	H	0	0	0	0
H	V	0	0	45	0
V	V	45	0	45	0
V	H	45	0	0	0
R	H	45	45	0	0
R	V	45	45	45	0
D	V	22.5	45	45	0
D	H	22.5	45	0	0
D	R	22.5	45	0	-45
D	D	22.5	45	22.5	-45
R	D	45	45	22.5	-45
H	D	0	0	22.5	-45
V	D	45	0	22.5	-45
V	L	45	0	45	-45
H	L	0	0	45	-45
R	L	45	45	45	-45
L	L	37	92	52	225

TABLE VI: Wave plates axes' inclination angles.

By performing the linear inversion procedure as explained in **Methods** section, the linear inversion density matrices $\hat{\rho}_{LI}$ ($\hat{\rho}_{LID}$ for the $|\phi_D\rangle$, $\hat{\rho}_{LI+}$ for the $|\phi^+\rangle$ and $\hat{\rho}_{LI-}$ for the $|\phi^-\rangle$) obtained are :

$$\hat{\rho}_{LID}=\begin{pmatrix} 0.4878 & -0.0541+0.0450i & -0.0350-0.0191i & 0.3013-0.0122i \\ -0.0541-0.0450i & 0.0344 & -0.0329+0.0057i & -0.0279+0.0594i \\ -0.0350+0.0191i & -0.0329-0.0057i & 0.0187 & 0.0245-0.0313i \\ 0.3013+0.0122i & -0.0279-0.0594i & 0.0245+0.0313i & 0.4591 \end{pmatrix}$$

$$\hat{\rho}_{LI+}=\begin{pmatrix} 0.4749 & -0.0632+0.0358i & -0.0402-0.0139i & 0.3481-0.0122i \\ -0.0632-0.0358i & 0.0290 & -0.0223+0.0057i & -0.0227+0.0542i \\ -0.0402+0.0139i & -0.0223-0.0057i & 0.0211 & 0.0337-0.0222i \\ 0.3481+0.0122i & -0.0227-0.0542i & 0.0337+0.0222i & 0.4749 \end{pmatrix}$$

$$\hat{\rho}_{LI-}=\begin{pmatrix} 0.4773 & -0.0624+0.0366i & -0.0374-0.0166i & -0.5037-0.0122i \\ -0.0624-0.0366i & 0.0283 & -0.0223+0.0057i & -0.0227+0.0542i \\ -0.0374+0.0166i & -0.0347-0.0057i & 0.0243 & 0.0329-0.0229i \\ -0.5037+0.0122i & -0.0255-0.0570i & 0.0329+0.0229i & 0.4701 \end{pmatrix}$$

In particular these matrices are:

- normalized $\longrightarrow Tr\{\hat{\rho}_{LI}\}$=1
- Hermitian $\longrightarrow \hat{\rho}_{LI} = \hat{\rho}_{LI}^{\dagger}$
- not positive semi-definite, in fact the eigenvalues do not exclusively consist of non-negative values:
  $\lambda_{\hat{\rho}_{LID}} = \{0.7804, 0.2215, -0.0250, 0.0227\}$,
  $\lambda_{\hat{\rho}_{LI+}} = \{0.8284, 0.1810, 0.0227, -0.0320\}$,
  $\lambda_{\hat{\rho}_{LI-}} = \{0.9864, 0.0781, 0.0121, -0.0767\}$.

Then the set of input values t_{inp} for the optimization process has been computed from each $\hat{\rho}_{LI}$. For instance for $\hat{\rho}_{LID}$ is equal to : t_{inp}={0.7531, 6.4077i, 0.1015, 0.6776, 0.6568, 0.0810, -0.2252, 1.3912, 0.0362, 0.0462, 1.9846, 2.6415, -0.0412, -0.0877, 0.4445, 0.0179}.
Suddenly the optimization algorithm has returned the optimal set of parameters t_{best} for (48). Again for example the $\hat{\rho}_{LID}$'s one is equal to : t_{best}={4.1989, -9.6594, 0.0196, 0.0040, 2.0505 -4.3251, -6.3958, 8.3801, -0.0141, 4.1544, 9.4822, 0.0508, -0.0046, -0.0041, -0.0012, 0.0006}.
Therefore, the obtained density matrices $\hat{\rho}_{LKL}$ ($\hat{\rho}_{LKLD}$ associated to $|\phi_D\rangle$, $\hat{\rho}_{LKL+}$ associated to $|\phi^+\rangle$ and $\hat{\rho}_{LKL-}$ associated to $|\phi^-\rangle$), computed using maximum likelihood estimation, can be expressed as follows:

$$\hat{\rho}_{LKLD}=\begin{pmatrix} 0.0501 & -0.0244-0.0516i & -0.0763+0.0999i & -0.0002+0.0495i \\ -0.0244+0.0516i & 0.3300 & -0.4003-0.0311i & -0.0510+0.0241i \\ -0.0763-0.0999i & -0.4003+0.0311i & 0.5709 & 0.0990-0.0752i \\ -0.0002-0.0495i & -0.0510-0.0241i & 0.0990+0.0752i & 0.0490 \end{pmatrix}$$

$$\hat{\rho}_{LKL+}=\begin{pmatrix} 0.0075 & -0.0268-0.0438i & 0.0194+0.0513i & -0.0000+0.0075i \\ -0.0268+0.0438i & 0.4679 & -0.4851-0.0704i & -0.0437-0.0269i \\ 0.0194-0.0513i & -0.4851+0.0704i & 0.5171 & 0.0511+0.0195i \\ -0.0000-0.0075i & -0.0437+0.0269i & 0.0511-0.0195i & 0.0075 \end{pmatrix}$$

$$\hat{\rho}_{LKL-}=\begin{pmatrix} 0.0195 & -0.0671+0.0802i & 0.0479-0.0608i & 0.0001+0.0196i \\ -0.0671-0.0802i & 0.6072 & -0.4612+0.0119i & 0.0805-0.0680i \\ 0.0479+0.0608i & -0.4612-0.0119i & 0.3535 & -0.0611+0.0486i \\ 0.0001-0.0196i & 0.0805+0.0680i & -0.0611-0.0486i & 0.0198 \end{pmatrix}$$

These matrices are:

- normalized $\longrightarrow Tr\{\hat{\rho}_{LKL}\}$=1
- Hermitian $\longrightarrow \hat{\rho}_{LKL}=\hat{\rho}^{\dagger}_{LKL}$
- positive semi-definite, in fact the eigenvalues do exclusively consist of non-negative values: $\lambda_{\hat{\rho}_{LKLD}}$=$\{0.9138, 0.0862, 0.2019\cdot10^{-7}, 0.4117\cdot10^{-6}\}$, $\lambda_{\hat{\rho}_{LKL+}}$=$\{0.9948, 0.0052, 0.1291\cdot10^{-4}, 0.5987\cdot10^{-3}\}$, $\lambda_{\hat{\rho}_{LKL-}}$=$\{0.9946, 0.0054, 0.6557\cdot10^{-5}, 0.3780\cdot10^{-2}\}$.

The Fidelity, Von Neumann entropy, and Concurrence values were computed as described earlier and recorded in Tab. VII. To estimate the errors associated with these quantities, a sample of 300 sets of coincidence counts was simulated, as described in the **Methods** section. The standard deviation was then calculated for the Fidelity, Von Neumann entropy, and Concurrence values obtained from these simulations.

$\hat{\rho}$	F	σ_F	S	σ_S	C	σ_C
$\hat{\rho}_{LID}$	0.2	0.4	0.885	0.001	0.621	0.003
$\hat{\rho}_{LKLD}$			0.423	0.005	0.907	0.008
$\hat{\rho}_{LI+}$	0.1	0.3	0.38	0.03	0.73	0.01
$\hat{\rho}_{LKL+}$			0.49	0.01	0.84	0.03
$\hat{\rho}_{LI-}$	0.1	0.4	0.79	0.02	0.66	0.01
$\hat{\rho}_{LKL-}$			0.48	0.01	0.84	0.03

TABLE VII: Fidelity, Von Neumann entropy, and Concurrence values with the associated statistical errors for the both type density matrices.

The Fidelity's value is pretty low meaning that the states are quite different and distant from each other, by the way the higher statistical error's value associated suggesting a meaningful uncertainty in the calculation. There could be several reasons for this high statistical error such that experimental noise on the data, the convergence of the optimization algorithm or the possible high variability of the simulated fidelities for instance. A way to improve the results could be perhaps collecting more data with less noise or increasing a lot the number of simulations.
The Von Neumann entropy is very high for $\hat{\rho}_{LID,LI-}$ and quite high for the others; this suggests a not well-defined quantum states and a considerable level of disorder. The statistical error is pretty low, proven the result's meaningful.
In conclusion the Concurrence is high for both type of density matrices, in particular for the $\hat{\rho}_{LKL}$s , suggesting a a remarkable degree of entanglement between the elements of the system (a bit smaller for $\hat{\rho}_{LI}$s but still meaningful). Also in this case the error is very low, indicating a good estimation of C.

Conclusions

During the final phase of the laboratory experiment, calculations were performed to determine the density matrix that represents the quantum state of light. Two different techniques were employed for this purpose. The outcome obtained through linear inversion, although affected by experimental noise, provided valuable insights. However, maximum likelihood estimation allowed for the extraction of a physically meaningful solution that closely approximates the result obtained through linear inversion. The Fidelity, Von Neumann and Concurrence have been computed for the obtained density matrices and simulations were conducted to estimate the statistical errors associated to these three quantities. Nonetheless, for a more precise estimation, considering the experimental errors associated with the inclination angles of the wave plate axes would be beneficial.

[1] James D.F.V., *et al.*, "On the Measurement of Qubits," Physical Review A, **64**, 05231 (2001). doi:10.1016/j.physrep.2019.03.001

[2] The explicit form of Pauli Matrices is: $\sigma_x=\begin{pmatrix}0&1\\1&0\end{pmatrix}$, $\sigma_y=\begin{pmatrix}0&-i\\i&0\end{pmatrix}$ and $\sigma_z=\begin{pmatrix}1&0\\0&-1\end{pmatrix}$.

[3] The results in (9),(10),(11), (12) could have been obtained also considering a state $\frac{1}{2}(|VV\rangle\langle VV|+|HH\rangle\langle HH|)$ which is separable.

[4] Note that they are the experimental equivalent of (13),(14),(15),(16).

[5] $\delta_f=\sqrt{(\frac{\partial f}{\partial x_1})^2\cdot\delta^2_{x_1}+...(\frac{\partial f}{\partial x_n})^2\cdot\delta^2_{x_n}}$ where $f(x_1,..,x_n)$ is a function depending on independent variables which are affected by an uncertainty $x_1\pm\delta_{x_1},...,x_n\pm\delta_{x_n}$.

[6] The explicit form of these operators is the following: $\hat{U}_{QWP}(q)=\frac{1}{\sqrt{2}}\begin{pmatrix}i-cos(2q)&sin(2q)\\sin(2q)&i+cos(2q)\end{pmatrix}$ and $\hat{U}_{HWP}(h)=\begin{pmatrix}cos(2h)&-sin(2h)\\-sin(2h)&-cos(2h)\end{pmatrix}$.
.

[7] Now $\hat{\rho}$ is definitely positive semidefinitive $\forall|\phi\rangle$: $||\hat{T}(t)|\phi\rangle||^2=\langle\phi|\hat{T}^{\dagger}(t)\hat{T}(t)|\phi\rangle\propto\langle\phi|\hat{\rho}(t)|\phi\rangle$